Chapter Seven:

Two Measurement Postscripts

This chapter discusses two further investigations which developed out of the experimental study of the corona wind in air and SF_6.

- When a length of optical fibre is heated, the optical path within the fibre changes because of changes in refractive index and in length. In general, these changes are not linear with temperature, they vary significantly with the material of the fibre and the rate of change of refractive index with temperature depends on wavelength. The thermal coefficients of silica optical fibres, due to changes in refractive index and linear expansion with temperature, have been measured for particular fibres at temperatures around room temperature (Hocker, 1979; Schuetz e*t al.*, 1983). However, in the present work, the temperature change induced in the optical fibre Fabry-Perot sensor (OFFPS) due to the heating of the fibre by a pulse from a carbon dioxide (CO_2) laser is as high as 800 °C. Therefore, it was decided to examine how the thermal coefficients of the fibre used here depend on temperature. This provides information on N, the fringe shift per degree per metre, which, in principle, could be used in the heat-balance equation for direct calibration of the OFFPS. Section 7.1 describes the experiment conducted to measure the thermal coefficients of the 3M single-mode 633 nm optical fibre over a range of temperatures above 75 °C.

- During the use of the OFFPS in a corona discharge in atmospheric air it was noted that the onset streamers were causing vibration of the fibre. Section 7.2 reports on the study undertaken into this phenomenon and presents a possible mechanism for this vibration.

7.1 High temperature calibration of an optical fibre

The optical fibre Fabry-Perot sensor (OFFPS) used to measure the speed of the corona wind in this work acted as a hot-fibre anemometer and, as such, relied on the variation of the refractive index and length of the fibre in response to a change in temperature. An estimate of the temperature reached by the fibre during heating by the CO_2 laser can be found by measuring the fringe shift on heating a known length of the fibre and using a documented value for the number of fringes per degree per metre N, in Equation 5.3, to find the temperature of the fibre.

The study described in this section developed out of the early experimental work on corona wind measurement using an optical fibre interferometer in a Michelson arrangement. The number of fringes recorded for a 200 ms heating pulse from the CO_2 laser was found to be as high as 180. For a CO_2 laser-beam diameter of 3.5 mm this number of fringes indicates a fibre temperature in excess of 1500 °C if the documented value of N = 17 fringes/deg/m for a silica fibre at room temperature is used (Hocker, 1979). A temperature of this magnitude would mean that the fibre was reaching temperatures very close to the softening point of silica (1670 °C - Weast, 1975). Since there was no evidence that the fibre was softening or melting and it is known that, in general, the thermal coefficients of bulk-glass materials do increase with temperature (Bååk, 1969), it became clear that N for the measuring fibre was increasing with temperature.

7.1.1 The thermal coefficient of a fibre

The phase response of a fibre to temperature has been outlined in Section 3.1.1 and Equation 3.3 is reproduced here as follows:

$$\frac{d\phi}{dT\,L} = \frac{2\pi}{\lambda}\left(\frac{n}{L}\frac{dL}{dT} + \frac{dn}{dT}\right) \tag{7.1}$$

where ϕ is the phase shift, T is the change in temperature, L is the length of affected fibre, λ is the wavelength of propagating light, n is the refractive index of the fibre, (dn/dT) is the thermal coefficient of refractive index and $[(dL/dT) / L]$ is the thermal coefficient of expansion.

In Equation 7.1, the refractive index, change in refractive index with temperature, and the coefficient of linear expansion, are all temperature dependent. Hocker used the following values in his calculation:

$$\frac{1}{L}\frac{dL}{dT} = 5 \times 10^{-7} \text{ /°C} \qquad \frac{dn}{dT} = 10 \times 10^{-6} \text{ /°C}$$

$$n = 1.456 \qquad \lambda = 0.6328 \times 10^{-6} \text{ m}$$

These parameter values are all for a temperature less than 100 °C and are values for pure silica. Whilst Hocker calculated the fringe coefficient of the fibre to be 17 fringes/deg/m, he obtained a value of 13.8 fringes/deg/m experimentally on heating a 1-m length of fibre over a temperature range of a few degrees around room temperature. Hocker attributed the discrepancy between the experimental and calculated values to doping of the fibre core, with the exact composition of the fibre unknown.

Optical fibre temperature sensors were among the earliest sensors developed using optical fibres, as they make use of the natural sensitivity of the fibre to changes in temperature. However, research in this area has tended to concentrate on the resolution (Musha *et al.*, 1982) and dynamic thermal response of the fibre (Schuetz *et al.*, 1983). The literature on the subject of thermal coefficients of optical fibres is surprisingly sparse, but a considerable amount of data is available for bulk optical materials. Bååk (1969) measured the thermal coefficients of refractive index and expansion for 23 Schott optical glasses at wavelengths of 435.8 nm, 546.1 nm and 632.8 nm over the temperature range of 25 to 75 °C, and for five of these glasses he extended the temperature range to 115 °C. For most of the glasses, Bååk found that both thermal coefficients varied by only a few percent over the given temperature range but, for a few of the glasses, the thermal coefficient of refractive index increased with temperature by up to 20% over the range of 35 to 115 °C. Bååk also noted that both positive and negative values of (dn/dT) occur and that glasses with a negative (dn/dT) tend to have the highest coefficient of thermal expansion.

White (1993) reviewed reference materials for calibration of dilatometers and included data on vitreous silica. Over a temperature range from 0 to 1000 °C, the thermal coefficient of expansion

was found to vary from 0.3 x 10^{-6} /deg to 0.5 x 10^{-6} /deg. White further noted that the thermal coefficient of expansion, in general, is insensitive to small changes in the chemical or physical purity of the glass, although, borosilicate glasses are an exception. Both White and Bååk conclude that not only the composition of the glass but also the mode of preparation of the glass is important for the values of the thermal coefficients.

The exact composition of an optical fibre is closely guarded by the manufacturer and to date we have been unable to secure any information concerning the composition of the optical fibres used in the experimental work on the corona wind speed. Thus, as a contribution to the study of thermal coefficients and in order to gain an understanding of the behaviour of optical fibres at high temperatures, an investigation of the thermal coefficients of refractive index and expansion for an unjacketed, single-mode, silica 3M optical fibre, designed for use at 633 nm, was performed. This wavelength is the same as that used by Hocker in his investigation and one of those used by Bååk.

7.1.2 Experimental arrangement

An optical fibre Fabry-Perot interferometer (OFFPI) was used to measure the fringe shift as a function of temperature, over a temperature range of 75 °C to 220 °C. The arrangement of the OFFPI is shown in Figure 7.1. The OFFPI was assembled from an ACROTEC 2x2, 633 nm single-mode, bidirectional coupler with a 110 mm length of 3M 633 nm single-mode optical fibre spliced to the cleaved end of one output arm, to form the resonant cavity of the interferometer. A conventional mechanical splice could not be used in this application as these have elements made from plastic materials which would not withstand the high temperatures. To splice the resonant cavity to the fibre coupler, quartz tubing was drawn so that a fine capillary was obtained. The internal diameter of the quartz capillary tube was 128 μm compared to the unjacketed fibre diameter of 125 μm. The output of the interferometer was monitored as the fibre ends were positioned in the capillary, so that a good quality resonant cavity was formed. The fibres were fixed in place with an epoxy resin which maintained its adhesive qualities to temperatures of 250 °C. The second arm of the coupler was terminated in an index-matching gel to eliminate reflections.

An electric furnace was used to heat the fibre. The furnace had an 80 mm-diameter ceramic insert which allowed access to the interior of the furnace. The fibre was placed in a 100 mm length of 3 mm inner-diameter copper tubing, which had five chromel-alumel thermocouples attached to it.

The copper tubing was wrapped in kao-wool to ensure that a constant temperature was reached over the length of the fibre. The copper tubing was connected to a glass tube which allowed the fibre to be moved in and out of the furnace without disturbing the positions of the thermocouples.

With the above arrangement the temperature of the fibre was monitored over the length of the resonant cavity whilst it was heated to temperatures around 200 °C. Throughout the experiment the readings on the thermocouples never differed by more than 1 °C. The output of the OFFPI was fed, via a photodetector, to a data acquisition board on a computer for later analysis. The outputs of the thermocouples in the furnace were connected to a direct-reading monitor and the output of the central thermocouple was amplified and also fed to the data acquisition board on the computer. Each measurement of fringe shift was made as the system cooled over a 4 °C range with the temperature of interest at the centre of the range; for example, for a data point at 150 °C, the system was cooled from 152 to 148 °C.

Due to the depreciation of the adhesive qualities of the epoxy resin at high temperatures, an optical fibre Michelson interferometer was used to obtain data above 200 °C. The reference arm of this interferometer was held in close contact with the sensing arm until the sensing arm entered the furnace. This ensured that the non-sensing fibre lengths of the interferometer were subject to the same environmental parameters, such as temperature and pressure, and extraneous optical path length differences between the interferometer arms were minimised.

7.1.3 The thermal coefficient of expansion

The fringe shift obtained with the above experimental arrangement is the total fringe shift due to both the thermal coefficients of refractive index and expansion. In order to separate the contributions of the two thermal coefficients to the total fringe shift, the expansion coefficient was measured separately. This was done by using low-coherence interferometry. This technique is discussed in Section 3.1.2, and the experimental arrangement is shown in Figure 7.2. A 42-mm length of unjacketed 3M single-mode 633 nm optical fibre was placed in a stainless steel capillary. One end of this fibre was fixed in position with epoxy resin and the other end was free to expand and contract with changes in temperature. The stainless steel tube was held in a ceramic holder which contained a heating element and thermocouple. The free-end of the fibre was cleaved and placed adjacent to a mirror so that an air-gap Fabry-Perot cavity was formed. Heating of the fibre caused the fibre to

lengthen and thus the air gap to narrow. Low-coherence interferometry allowed the absolute gap width, and hence the change of the fibre length, to be measured as a function of temperature.

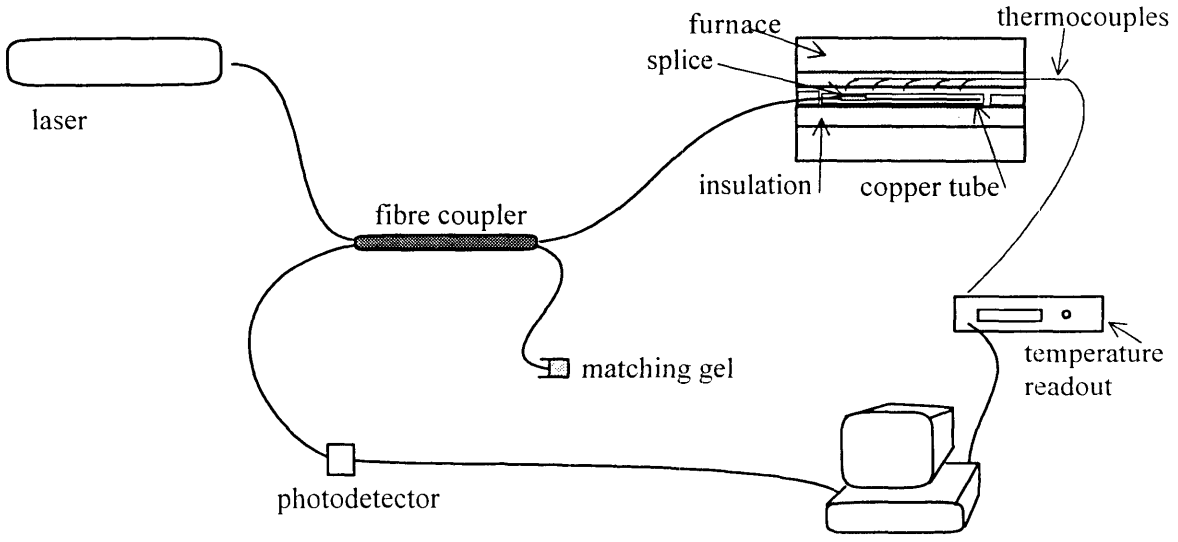

Figure 7.1 Experimental arrangement for the measurement of the fringe coefficient N as a function of temperature.

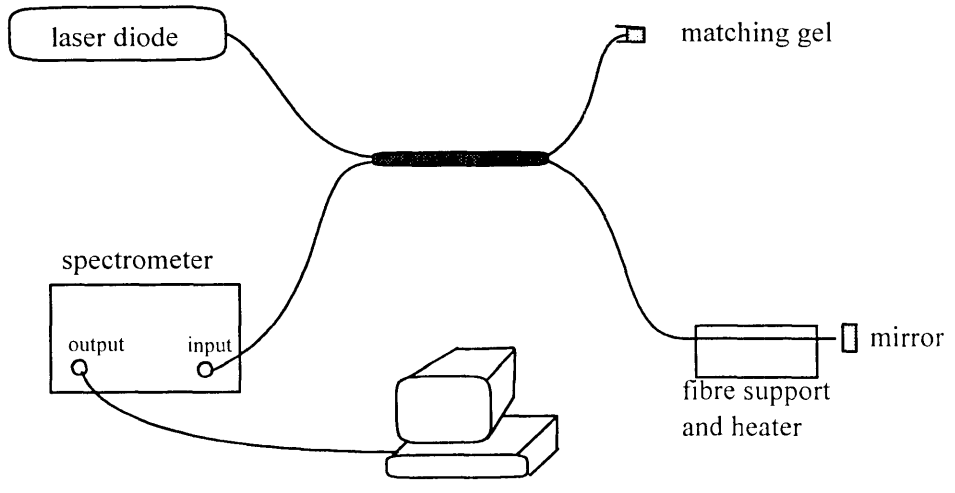

Figure 7.2 Optical arrangement for the measurement of thermal expansion of an optical fibre.

The low-coherence optical source for the interferometer was a Toshiba 9211.144 multimode laser diode, with a central wavelength of 672 nm and bandwidth of 17 nm. The interferometric signals were processed using the channelled-spectrum technique, where changes in the optical path difference of the sensing interferometer are determined by monitoring the cavity free spectral range by dispersing the light from the sensing interferometer with a diffraction grating onto a CCD array (Taplin *et al.*, 1994).

7.1.4 Results and discussion

Figure 7.3 is a graph of the total fringe shift/deg/m (or fringe coefficient) as a function of temperature, obtained using the arrangement of Figure 7.1. The curve is linear with the fringe coefficient increasing at a rate of 0.044 fringes/deg/m per degree. The data points taken with the Michelson optical fibre interferometer are slightly higher than those obtained with the OFFPS but they have the same gradient. The data extrapolate linearly to a value of 16.3 fringes/deg/m at 20 °C and this agrees with the experimental value which was obtained at room temperature. The linear nature of the change in the fringe coefficient is similar to that found by Bååk (1969) for some bulk glasses, although the rate of increase for the fibre is substantially greater.

The data for the contribution of the linear expansion coefficient to the overall fringe shift are shown in Figure 7.4 where the width of the air Fabry-Perot gap is plotted as a function of temperature. The linearity indicates that there is little change in the thermal coefficient of expansion with temperature over the range 25 °C to 215 °C. The line of best fit through the data gives a value of 1.8×10^{-6} /deg for this coefficient. This value is higher than that of 0.4×10^{-6} /deg quoted by White (1993) for pure fused silica. As mentioned earlier, the composition of the 3M fibre is unknown and the high value of the thermal coefficient of expansion may be due to the doping level of the fibre.

The measurements of the linear-expansion and refractive-index thermal coefficients were made at wavelengths of 672 nm and 633 nm respectively, but since the linear expansion coefficient does not depend on wavelength, the contribution due to thermal expansion can be subtracted from the overall fringe shift to give a value for the refractive-index thermal coefficient (dn/dt) at 633 nm. The value of dn/dt was found to increase linearly from 7.7×10^{-6} /deg at 20 °C to 13.5×10^{-6} /deg at 220 °C. This compares to an average value of 12.9×10^{-6} /deg for bulk fused silica measured by Toyoda and Yabe (1983), at the same wavelength over the range from room temperature to 400 °C.

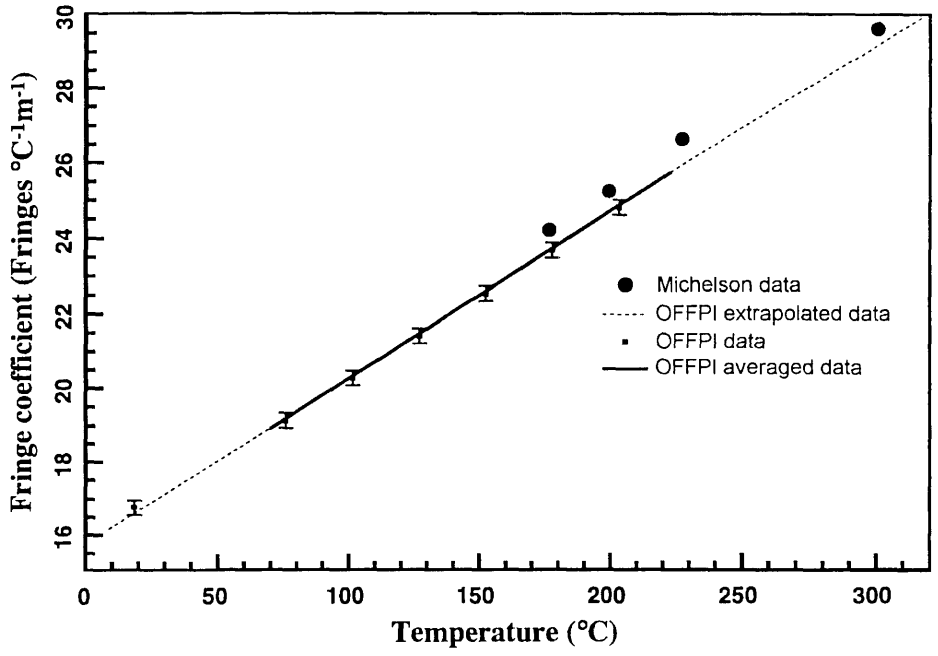

Figure 7.3 Total fringe shift/deg/m for the OFFPI and the Michelson interferometer.

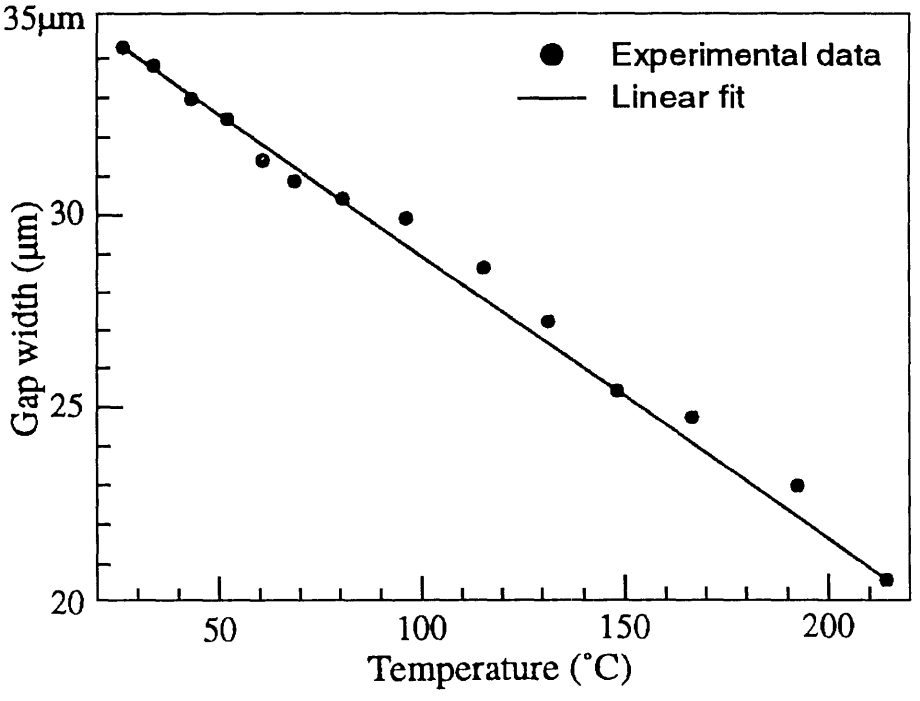

Figure 7.4 Absolute fibre-mirror gap for the measurement of the thermal linear-expansion coefficient.

The results presented here are for a particular single-mode fibre manufactured by 3M, at a wavelength of 633 nm. The results of this experiment and of those using bulk glasses show that the nature of the variation with temperature of the thermal coefficients is critically dependent on the type of glass. This highlights the need for calibration of any optical fibre interferometric sensor, where it is to be used for absolute measurement, either when temperature is the measurand of interest or where temperature needs to be taken into account, as for example, in an interferometric sensor used for flow measurement.

7.2 The effect of onset streamers on the optical fibre sensor

A corona discharge is established when a high potential is applied between electrodes in a non-uniform field distribution. Prior to onset of a self-sustained discharge, increasing the potential on the point electrode causes the corona current to go through a period of erratic behaviour called the 'burst pulse' or 'onset streamer' regime. Section 2.1.1 has described this process in detail. During the investigation of the corona wind it was noted that the optical fibre Fabry-Perot sensor (OFFPS) was responding to these onset streamers. Onset streamers typically take the form of a pulse of current and light known as the primary pulse. This may be followed by a series of smaller, secondary pulses (Sigmond, 1983). Figure 7.5 is a trace of the fringes seen on the OFFPS due to three onset streamers in atmospheric air. The primary streamer is seen to cause the largest disturbance of the fibre with a maximum fringe shift of the order of one fringe. Figure 7.6 shows a typical current pulse due to an onset streamer.

Direct observation of the fibre indicted that the fringe shift is caused by fibre vibration which stretches the fibre to produce an oscillating fringe shift as a result of the changing optical path length. The primary pulse seen in Figure 7.5 produced a fringe shift of one fringe and this is equivalent to a transverse movement of around 0.2 mm away from the equilibrium fibre position.

There are several mechanisms which could account for this disturbance of the fibre and its resultant vibration within the discharge gap;

- *Corona-wind pulses:*
  Streamers propagate across the corona gap at some 10^5 m/s and following the streamer current pulse the positive ions transfer their momentum to the neutral gas molecules producing a pulse of

corona wind along the axial direction. Tajalli *et al.* (1989) measured the corona wind associated with these streamers by the Schlieren technique and found it to have speeds between 8 m/s and 12 m/s in air.

- *Radial shock-front*:
  Electron - neutral elastic collisions occur during the streamer propagation and these generate a radial shock-front which moves radially outwards at around 350 m/s in air (Tajalli *et al.*, 1989).
- *Ionic charging of the fibre:*
  Charging of the fibre by ions produced in the streamer and consequent electrostatic forces on the fibre could cause vibration of the fibre.

In order to determine which of these possibilities was causing the fringes to occur on the OFFPS, the fringe traces and the initiating current pulses were examined using a LeCroy 9410 Dual-Channel digital oscilloscope. The experimental arrangement of the discharge chamber and the OFFPS was the same as for the experimental work on the corona wind in atmospheric air and is described in Chapter 4. The fibre was positioned mid-gap unless otherwise stated.

7.2.1 Results and discussion

The fringes were found to have a frequency of around 60 Hz at all times and this was independent of the amplitude of the current pulse. Vibration of the fibre by either knocking the table on which the discharge chamber was situated or blowing gently on the fibre produced fringes of the same frequency. Therefore, the frequency of 60 Hz is the natural vibration frequency of the length of fibre suspended across the discharge chamber.

The time delay between the appearance of the fringe trace and that of the current pulse was less than a microsecond and furthermore, the position of the fibre within the discharge gap made no significant difference to the time delay. These two results combine to effectively rule out the corona wind as being the instigator of the signal on the OFFPS, as the relatively slow speed of the corona wind would be seen as a time delay between the current pulse and the fringe signal and this time delay should lengthen as the fibre is moved away from the anode.

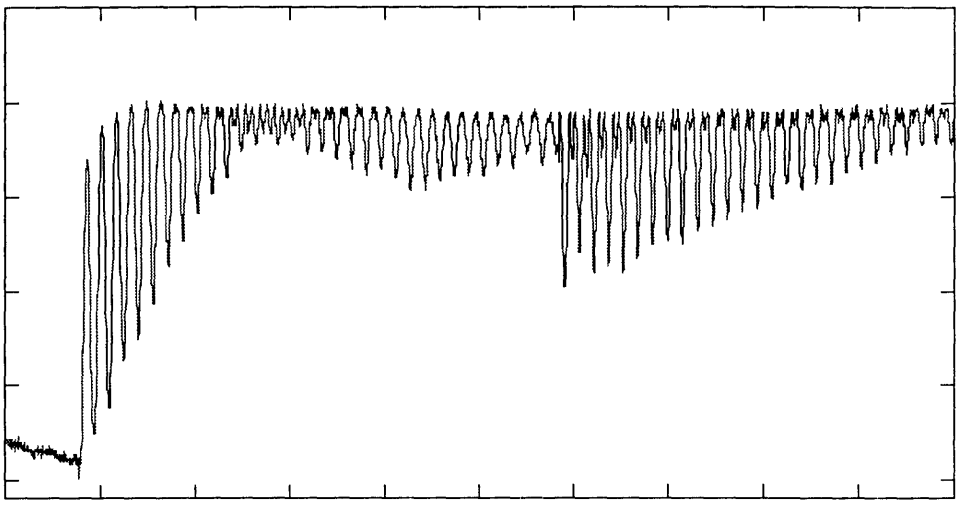

Figure 7.5 Fringe trace showing OFFPS response to a burst of streamers. Time base 0.2 sec/div.

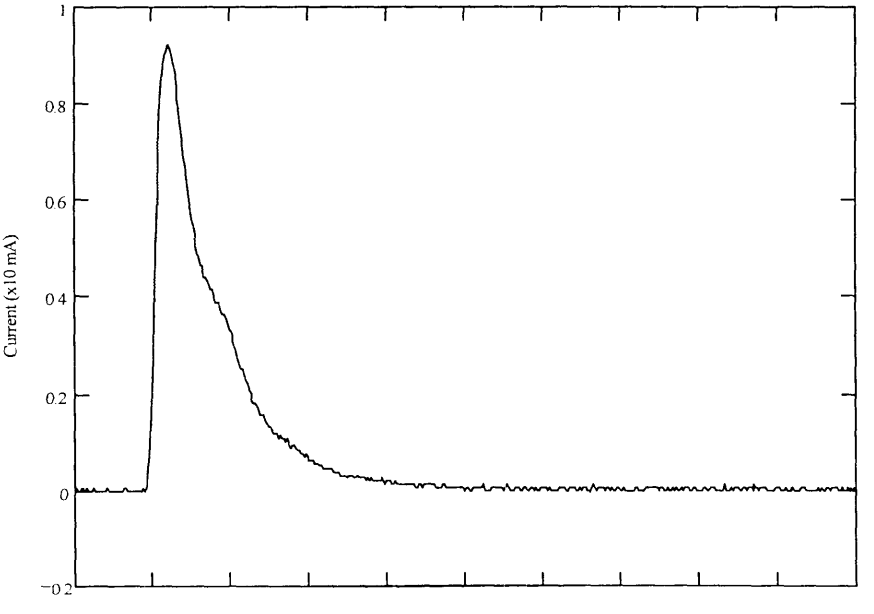

Figure 7.6 Current pulse due to an onset streamer. Time base 0.5 μsec/div.

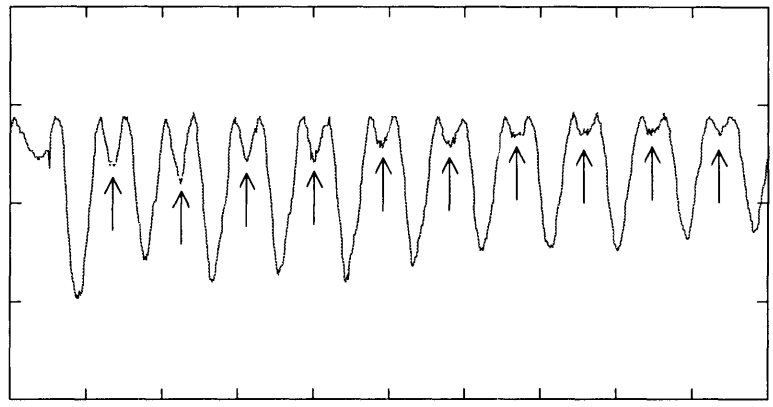

Figure 7.7 Expanded view of the streamer signal from the OFFPS - arrows indicate the turnaround points in the fringe pattern. Time base 35 ms/div.

When the plane electrode was replaced by a grounded grid and the fibre positioned directly under the grid the signal on the OFFPS disappeared. Since the corona wind represents a movement of neutral molecules, its effect should still have been observed. Since, the shock-front moving away from the streamer head is also a movement of neutrals it is reasonable to assume that its effect would not cease at the grid but be felt some distance below the grid. As no signal was seen with the fibre directly below the grid the shock-front was discounted as the initiating mechanism. On the other hand, the fibre is shielded from ionic effects. Therefore, it appears that the signal on the OFFPS is caused by charging of the fibre in the presence of the short-lived onset streamers.

The fibre was viewed with a microscope as the voltage on the point electrode was increased, and prior to the onset of any corona activity, the fibre was observed to move towards the region of high electric field, that is, towards the point. This is due to polarisation of the fibre by the applied field. When onset streamers occur, they inject pulses of positive charge into the corona gap. This charge is attracted to the negative surface of the fibre, which is nearest the point, and the net result is an impulse causing the fibre to move rapidly towards the cathode. An elastic restoring force, modified by a varying electrostatic force, produces damped oscillations until the fibre returns to an equilibrium position. Figure 7.5 shows these damped oscillations as the amplitude of the signal decreases with time. Figure 7.7 is an expanded view of the OFFPS streamer signal and the oscillatory nature of the motion is clear. The trace shows the decreasing amplitude of the fibre vibration over time and the arrows indicate the points at which the fibre reaches its maximum excursion from the equilibrium position and begins to move in the opposite direction.

Chapter Eight:

Summary and Conclusions

This thesis has set out to provide information on the speed of the corona wind and its three-dimensional profile in both atmospheric air and SF_6 coronas. Electrical coronas require diagnostic techniques which cause a minimum amount of perturbation of the discharge conditions and optical methods meet this requirement. Optical fibres are ideal for use in electrical discharges as their dielectric nature ensures that disturbance of the electric field is minimised at all positions within the discharge gap, except very close to the point electrode. Charging of the fibre, due to the presence of positive ions within the discharge gap, was noted but is not important in this study as the corona wind constitutes a flow of neutrals.

An optical fibre sensor was developed which utilised a fibre Fabry-Perot interferometer as a sensing element within the corona. The flow of the corona wind over a heated section of the interferometer resulted in a fringe shift which related to the wind speed. The corona wind speed in air was also measured using the conventional flow measurement technique of laser Doppler anemometry (LDA). LDA has limitations as a flow measurement technique within corona discharges as it requires the presence of particles, and these particles become charged so that they move due to the combination of an electrostatic force and the action of the corona wind. The comparison between the LDA results and the optical fibre Fabry-Perot sensor (OFFPS) results provides information on the charging of

particles within the corona and the speed of these particles due to the corona wind alone. Both the optical fibre and LDA techniques were successfully applied to measurement of the corona wind speed in air, and optical fibre sensing was successfully used to measure, for the first time, the speed of the corona wind in SF_6.

The study of electrical coronas in gases is important because of their many applications. Intentionally generated coronas are used in many industrial areas, such as photocopiers, laser printers and electrostatic precipitators. However, unwanted coronas are a problem for the electrical power industry where coronas in high-voltage gas-insulated systems can damage the structure and ultimately lead to the failure of the system. The corona wind is a phenomenon which is always present in a corona discharge. The corona wind has found a role in the enhancement of heat and mass transfer from a heated surface, by providing a small localised jet for cooling. This application has been extended to include the use of the corona wind to assist the even distribution of heat in commercial ovens and for putting out fires in flammable liquids. Of particular interest is the role of the corona wind in practical systems where coronas are utilised, as little work has been done on the interaction of the corona wind with other corona electrical and physical characteristics.

A complete understanding of corona discharges is required in the electrostatic precipitation process which relies on the charging of particulate matter in a corona discharge and its subsequent movement due to the presence of the corona electric field. As mentioned earlier, the movement of the particulate matter is determined by both electrostatic forces and the corona wind. Precipitator efficiencies of the order of 99.5 % are presently required by many governing bodies and with the tightening of environmental controls on industry it is imperative that a complete understanding of the many processes within electrostatic precipitators is gained. One of the factors affecting the efficiency of an electrostatic precipitator is the interplay of the corona wind with the flow of exhaust gas through the precipitator. The optical fibre sensor developed as part of this work has been successfully employed to measure the speed of the corona wind within a laboratory precipitator (Scelsi *et al.*, 1996). The combination of information from the optical fibre sensor and LDA can be used to separate the relative contributions of the corona wind and the electrostatic forces to the speed of the particulate matter. Results from the present work suggest that the corona wind may make a significant contribution to the speed of the particulate matter. Thus, the combination of LDA and optical fibre sensing provides useful information about the process of electrostatic precipitation, and knowledge of the corona wind profile can be used to map the complete flow of exhaust gas through the precipitator.

Coronas occurring within high-voltage gas-insulated systems, especially those that use sulphur hexafluoride (SF_6) as the insulating gas, are extremely important. Knowledge of the profile of the corona wind speed in SF_6 is vital for the understanding of the interactions within an SF_6 corona and can be used in conjunction with established discharge data to complete the picture of SF_6 coronas. Coronas in SF_6 cause dissociation of the SF_6 which leads to the build up of decomposition products on the surfaces of the system. The action of the corona wind within the SF_6 system will affect both the recombination of the SF_6 and the distribution of solid by-products throughout the device. Thus, quantitative data on the corona wind in SF_6 can contribute to design optimisation of these high-voltage gas-insulated systems.

The experimental results for the corona wind speed compare favourably with predictions based on electrohydrodynamic theory. The roles of the corona current and the physical configuration of the electrode system were also found to broadly agree with theory. This investigation has produced the first-ever measurement of the speed and three-dimensional speed profile of the corona wind in an SF_6 corona discharge. The speed of the corona wind in SF_6 was found to be lower than the speed of the corona wind in air by a factor of 4 to 5, which is consistent with theoretical predictions. In order to completely understand the effect of corona electrical parameters on the corona wind, diagnostic techniques which allow measurement of parameters such as local electric field and charge density within the corona gap are required and optical fibre sensors are being developed for this purpose (Priest *et al.*, 1997).

Many streams of future research suggest themselves from this study of the corona wind using the optical fibre Fabry-Perot sensor (OFFPS). The OFFPS has potential as a diagnostic tool in any flow system, especially those that occur within electromagnetically noisy environments. There is a wide range of coronas in which the corona wind is yet to be investigated, such as negative coronas, ac coronas and coronas in different gases and gas mixtures at different gas pressures. Monitoring high-voltage gas-insulated systems is a subject of much research and a simple corona monitor which can be used in the field is still being sought. The OFFPS developed for this study was found to be remarkably sensitive to the presence of coronas in SF_6 at pressures above 30 kPa. Further investigation into the distance from the point of corona formation, over which the sensor remains sensitive in high-pressure SF_6 systems, could ultimately lead to the development of a corona monitoring device which utilises optical fibre technology.